

Real Active Site Identification of Co/Co₃O₄ Anchoring Ni-MOF Nanosheets with Fast OER Kinetics for Overall Water Splitting

Haoran Yin, Xinqiang Liu, Lixia Wang, Tayirjan Taylor Isimjan,* Dandan Cai,* and Xiulin Yang*

Cite This: *Inorg. Chem.* 2024, 63, 7045–7052

Read Online

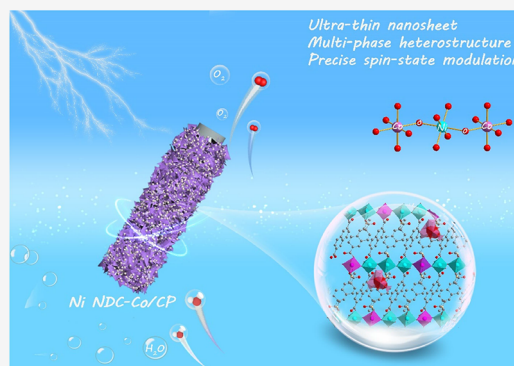
ACCESS |

Metrics & More

Article Recommendations

Supporting Information

ABSTRACT: Doping metals and constructing heterostructures are pivotal strategies to enhance the electrocatalytic activity of metal–organic frameworks (MOFs). Nevertheless, effectively designing MOF-based catalysts that incorporate both doping and multiphase interfaces poses a significant challenge. In this study, a one-step Co-doped and Co₃O₄-modified Ni-MOF catalyst (named Ni NDC-Co/CP) with a thickness of approximately 5.0 nm was synthesized by a solvothermal-assisted etching growth strategy. Studies indicate that the formation of the Co–O–Ni–O–Co bond in Ni NDC-Co/CP was found to facilitate charge density redistribution more effectively than the Co–O–Ni bimetallic synergistic effect in NiCo NDC/CP. The designating Ni NDC-Co/CP achieved superior oxygen evolution reaction (OER) activity (245 mV @ 10 mA cm⁻²) and robust long stability (100 h @ 100 mA cm⁻²) in 1.0 M KOH. Furthermore, the Ni NDC-Co/CP⁽⁺⁾||Pt/C/CP⁽⁻⁾ displays pregnant overall water splitting performance, achieving a current density of 10 mA cm⁻² at an ultralow voltage of 1.52 V, which is significantly lower than that of commercial electrolyzer using Pt/C and IrO₂ electrode materials. In situ Raman spectroscopy elucidated the transformation of Ni NDC-Co to Ni(Co)OOH under an electric field. This study introduces a novel approach for the rational design of MOF-based OER electrocatalysts.



INTRODUCTION

Green hydrogen, considered the most promising future energy, is currently produced mainly by electrolyzing water.^{1,2} However, the efficiency of electrocatalytic water splitting faces challenges due to the anodic oxygen evolution reaction (OER), involving a complex four-electron transfer process with sluggish reaction kinetics.^{3,4} Typically, noble metal catalysts like Ru/Ir are widely employed for OER, but their high cost and scarcity hinder widespread application.^{5,6} Therefore, the pursuit of alternative electrocatalysts with comparable OER activities yet lower cost and higher abundance has become a compelling research focus. Over recent decades, transition-metal materials have emerged as promising candidates due to their flexible oxidation states, variable d-orbital electronic structures, cost-effectiveness, and diversity. This has led to the development of numerous transition-metal-based electrocatalysts, including transition-metal oxides, phosphides, sulfides, and others.^{7–9}

Among the above-mentioned electrocatalysts, metal–organic frameworks (MOFs), recognized as typical porous coordination polymers, have garnered considerable attention due to their distinctive coordination environment, expansive surface area, and tunability.^{10,11} However, pristine MOFs encounter challenges such as poor electrical conductivity and restricted active metal centers, limiting their application as efficient OER electrocatalysts.^{12–14} To address these limitations, researchers have undertaken extensive efforts to

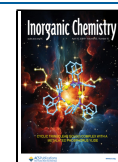
enhance the electrocatalytic activity of MOFs through methods such as element doping, defects construction, and morphology engineering.^{15–17} Notably, doping with foreign elements stands out as an effective approach, capitalizing on electronic interactions and cooperative effects between metal centers.^{18,19} For instance, Zhao et al. demonstrated the high OER performance (250 mV@10 mA cm⁻²) of a NiCo MOF, attributing it to the electronic interaction between Ni and Co, which optimized their OER performance.²⁰ Moreover, the combination of MOFs with other active metals or metal oxides has proven to exhibit superior electrocatalytic activity compared to individual components.^{21–23} Zheng et al. synthesized a Co₃O₄@Co MOF, showcasing a synergistic effect that enhanced OER ability (277 mV@10 mA cm⁻²).²⁴ Importantly, while doping with other metals modulates the electronic structure of the initial MOF, hybridization with metallic materials creates interfaces to optimize electron transfer.^{25–27} As of now, formulating a viable strategy to

Received: February 19, 2024

Revised: March 20, 2024

Accepted: March 20, 2024

Published: April 3, 2024



combine doping and compositing for maximal MOF modification remains a significant challenge.

Motivated by these considerations, Co_3O_4 -modified and Co-doping Ni MOF (Ni NDC-Co/CP) was prepared through a solvothermal-assisted etching growth strategy. In comparison to NiCo NDC/CP, Ni NDC-Co/CP demonstrates superior OER activity of 245 and 308 mV at 10 and 100 mA cm^{-2} , respectively, while maintaining stability for 100 h at 100 mA cm^{-2} . When Ni NDC-Co/CP⁽⁺⁾||Pt/C/CP⁽⁻⁾ cells were assembled, low voltages of 1.52 and 1.63 V were attained at 10 and 100 mA cm^{-2} , respectively, with stability sustained for over 70 h at 100 mA cm^{-2} . Comprehensive characterizations confirmed that the outstanding electrocatalytic performance of Ni NDC-Co/CP originates from the Co–O–Ni–O–Co bond, resulting from the cooperative effects of Co doping and Co_3O_4 modification. In situ Raman results further corroborate the transformation of Ni NDC-Co into Ni(Co)-OOH as the real active component in the electrochemical reaction.

RESULTS AND DISCUSSION

The preparation process of Ni NDC-Co/CP is shown in Figure 1. Initially, the pristine 2D Ni NDC with a MOF

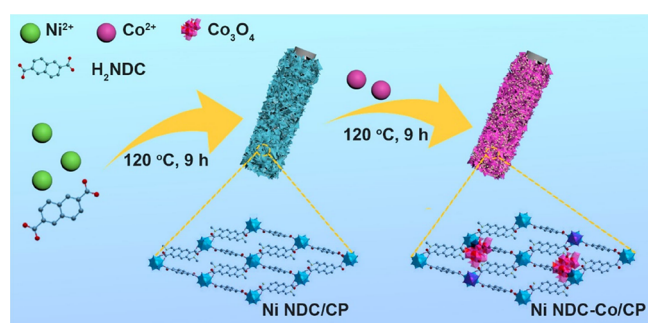


Figure 1. Schematic illustration of the synthesis of Ni NDC-Co/CP.

coordination environment was synthesized using a straightforward one-step solvothermal strategy, employing $\text{NiCl}_2 \cdot 6\text{H}_2\text{O}$ and H_2NDC as the metal source and organic ligand, respectively. In the subsequent ion etching growth process, Co^{2+} was effectively introduced into the second building units of Ni NDC, facilitated by the presence of the same six Co/Ni coordination centers.^{28,29} Concurrently, a portion of the Co^{2+} ions underwent oxidation, forming Co_3O_4 , which intricately decorated the surface of Ni NDC nanosheets, leading to the self-regulated formation of the Ni NDC-Co/CP heterostructure.

X-ray diffraction (XRD) was employed to scrutinize the crystal structures of the catalysts. In Figure 2a, all samples displayed the characteristic peaks at 26.6 and 54.8°, assignable to the background CP (PDF# 26–1077).³⁰ Notably, Ni NDC/CP, NiCo NDC/CP, and Ni NDC-Co/CP displayed two similar peaks at 7.5 and 14.8°, aligning well with the (001) and (002) facets of the Ni MOF simulation, affirming the successful construction of NDC-based MOF composites.^{28,31} Intriguingly, the XRD pattern of the Ni NDC-Co/CP catalyst did not reveal any Co_3O_4 diffraction peaks, in contrast to clear peaks observed in samples collected at the bottom of the solvent thermal reactor (Figure S1), indicating the low-loading Co_3O_4 modification in the target catalyst.^{32,33} Raman spectroscopy was performed to further explore the characteristic

peaks of Ni NDC/CP, NiCo NDC/CP, and Ni NDC-Co/CP (Figure 2b). Obviously, the peaks in the range of 1300 to 1800 cm^{-1} correspond to the characteristics of H_2NDC organic ligands, and the peak at 668 cm^{-1} is attributed to the characteristic peak of M–O bonds, once again verifying the sufficient coordination of metal ions and organic ligands.^{34–36} Compared to Ni NDC/CP and NiCo NDC/CP, Ni NDC-Co/CP exhibited new peaks at around 470, 680, and 1180 cm^{-1} , indicating the presence of Co_3O_4 species.³⁷

The morphology and structure of the samples were characterized by scanning electron microscopy (SEM). Remarkably, Ni NDC/CP presents cross-linked nanosheets with smooth surfaces (Figure 2c). For NiCo NDC/CP, the nanosheets were slightly overlapped and thicker than those of Ni NDC (Figure S2). In the case of Ni NDC-Co/CP, the apparent surface roughness of the nanosheets can be explained by the decoration of Co_3O_4 , which validates the previously explained ion etching growth mechanism (Figure 2d). Atomic force microscopy (AFM) test results show that Ni NDC-Co retained its ultrathin properties with a thickness of about 5.0 nm (Figure 2e). Transmission electron microscopy (TEM) images in Figure 2f also validated the nanosheet structure, with clear lattice fringes and plane spacing of 0.24 and 0.58 nm observed in the high-resolution TEM (HR-TEM) image, attributed to the (311) and (002) planes of Co_3O_4 and Ni NDC, respectively (Figure 2g). Additionally, the selective area electron diffraction (SAED) pattern in Figure 2h revealed diffraction rings corresponding to the (311) plane of Co_3O_4 and the (002) plane of Ni NDC, consistent with the lattice fringes in Figure 2g. The corresponding EDX spectra showcased a homogeneous distribution of O, Ni, and Co, while ICP-MS further clarified the elemental content of Ni (8.87 wt %) and Co (6.18 wt %) (Figure 2i, Table S1).

The elemental valences of Ni NDC/CP, NiCo NDC/CP, and Ni NDC-Co/CP were scrutinized using X-ray photoelectron spectroscopy (XPS). Specifically, the C 1s binding energy in the original data was standardized to 284.8 eV, and subsequently, the high-resolution Ni 2p and Fe 2p XPS spectra were analyzed by using peak splitting rules. The XPS survey spectra of various catalysts exhibit the presence of O, Ni, and Co elements concurrently (see Figure S4), consistent with the findings of EDS mapping. In the Ni 2p spectra (Figure 3a), the peak at 858.25 eV corresponds to the typical Ni^{3+} species, while the peak at 856 eV belongs to the Ni^{2+} state.^{38–40} For Co 2p spectra (Figure 3b), the peaks of Co^{2+} can be observed with the binding energy of 781.3 ($\text{Co}^{2+} 2p_{3/2}$), and the peaks at 780.1 eV can be ascribed to the $\text{Co}^{3+} 2p_{3/2}$.^{41,42} The relative ratio of $\text{Ni}^{3+}/\text{Ni}^{2+}$ is higher in Ni NDC-Co/CP compared to NiCo NDC/CP, suggesting a greater proportion of high-valence Ni^{3+} in Ni NDC-Co/CP. This phenomenon is advantageous for the OER process.^{43,44} Additionally, the binding energy of Ni^{2+} in Ni NDC-Co/CP and NiCo NDC/CP is more positively shifted than in Ni NDC/CP, implying a localized alteration in the electronic environment of Ni^{2+} .⁴⁵ Considering the dual effect of Co doping and Co_3O_4 modification in Ni NDC-Co/CP and the XPS results, a Co–O–Ni–O–Co bond is proposed based on the crystal field theory to describe the electron-transfer mechanism present in Ni NDC-Co/CP (Figure 3c). In Ni NDC/CP, the π -symmetry d -orbitals (t_{2g}) of the Ni^{2+} are fully occupied, resulting in the e^- – e^- repulsion as the main interplay of the bridging O^{2-} and Ni^{2+} .⁴⁶ The symmetrically filled electronic degenerate orbitals (e_g and t_{2g}) of Ni^{2+} prevent Jahn–Teller (JT) distortion,

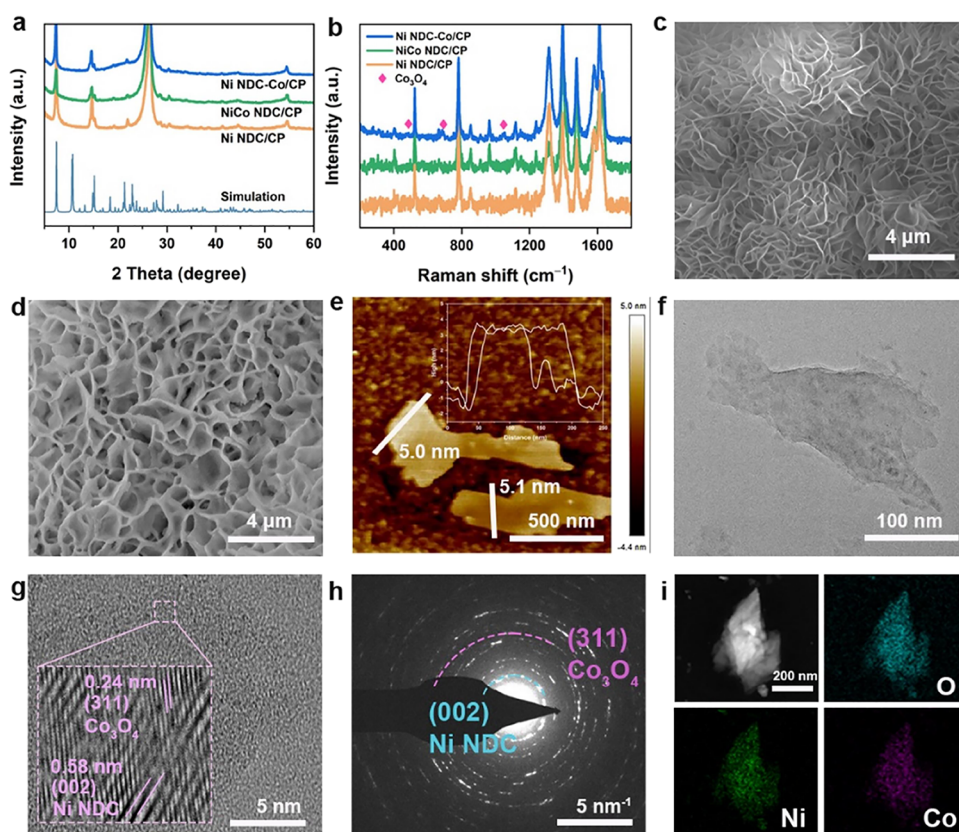


Figure 2. (a) XRD patterns of Ni NDC/CP, simulated Ni NDC, NiCo NDC/CP, and Ni NDC-Co/CP. (b) Raman patterns of Ni NDC/CP, NiCo NDC/CP, and Ni NDC-Co/CP. (c) SEM image of the Ni NDC/CP. (d) SEM image, (e) AFM image, (f) TEM image, (g) HR-TEM image, (h) SAED image, and (i) EDS mapping of Ni NDC-Co/CP.

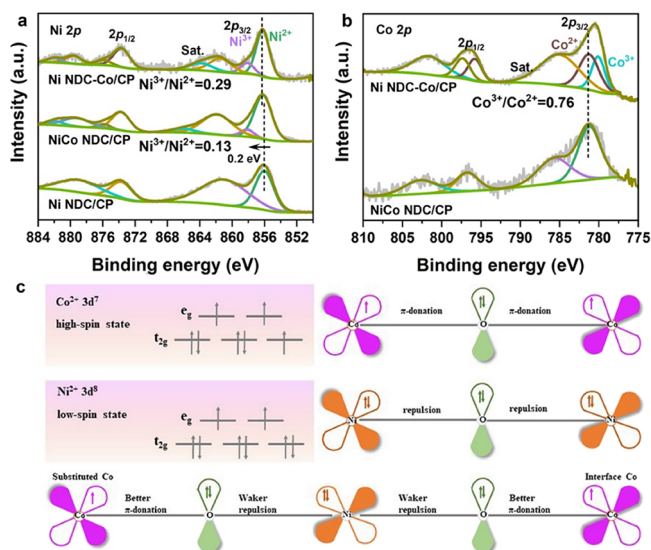


Figure 3. (a) High-resolution Ni 2p XPS spectra of Ni NDC/CP, NiCo NDC/CP, and Ni NDC-Co/CP; (b) Fe 2p XPS spectra of NiCo NDC/CP and Ni NDC-Co/CP; and (c) schematics of the electronic interplay among Ni NDC-Co/CP.

requiring a high input energy for the OER to proceed.⁴⁷ In contrast, the electronic valence configuration of Co^{2+} is $3d^7$ with the high-spin state, leading to unpaired electrons in the π -symmetric (t_{2g}) d-orbitals that interact with the bridging O^{2-} through π -donation.⁴⁸ Through dual modification of Ni^{2+} from two Co^{2+} molecules at both sides via $\text{Co}-\text{O}-\text{Ni}-\text{O}-\text{Co}$,

stronger electron transfer occurs, transforming Ni^{2+} ($t_{2g}^6 e_g^2$) to Ni^{3+} ($t_{2g}^6 e_g^1$). Notably, Ni^{3+} exhibits JT distortion due to the asymmetric filling of electronic degenerate orbitals, favoring the OER.⁴⁹ Overall, Co, as an electron acceptor, extracts electrons from the Ni site through the $\text{Co}-\text{O}-\text{Ni}-\text{O}-\text{Co}$ electronic coupling effect, converting Ni^{2+} to Ni^{3+} , resulting in JT distortion, shortening of Ni–O bonds, and improved OER activity.^{50,51}

The OER activity of the variously prepared catalysts was assessed by a three-electrode measurement system in 1.0 M KOH, and all linear sweep voltammetry (LSV) curves were calibrated with 95% iR compensation. Given that the $\text{CoCl}_3 \cdot 6\text{H}_2\text{O}$ content significantly influences catalytic performance, Ni NDC-Co/CP obtained by adding different mmol of $\text{CoCl}_3 \cdot 6\text{H}_2\text{O}$ was initially evaluated for the OER activity. The results indicated that the optimal amount of $\text{CoCl}_3 \cdot 6\text{H}_2\text{O}$ was 1.5 mmol (Figure S3). In Figure 4a, Ni NDC-Co/CP exhibits an overpotential of 245/308 mV at a current density of 10/100 mA cm^{-2} , surpassing those of other samples. Overpotentials at current densities of 10, 50, and 100 mA cm^{-2} were used as comparative variables, with the relative results presented in Figure 4b. The kinetics of the OER process were further evaluated by Tafel slopes.⁵² Notably, the Tafel slope of Ni NDC-Co/CP (49.1 mV dec^{-1}) is significantly lower than that of Ni NDC/CP (105.5 mV dec^{-1}), NiCo NDC/CP (53.2 mV dec^{-1}), and RuO_2/CP (186.3 mV dec^{-1}), indicating faster OER dynamics for Ni NDC-Co/CP (Figure 4d). Importantly, Ni NDC-Co/CP competes favorably with recently reported OER catalysts (Figure 4c, Table S2). The electrochemical active surface area (ECSA) value is a crucial factor reflecting

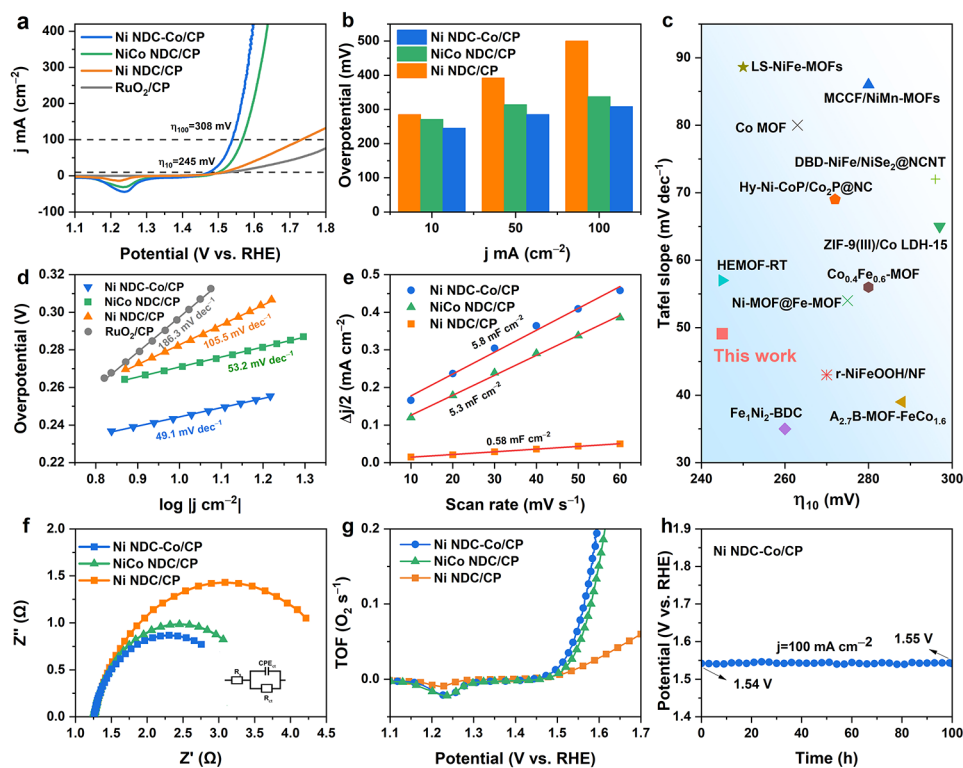


Figure 4. (a) Linear sweep voltammetry (LSV) curves of Ni NDC-Co/CP, NiCo NDC/CP, Ni NDC/CP, and RuO₂/CP in the OER. (b) Overpotentials for different samples at 10, 50, and 100 mA cm⁻². (c) Comparison of the overpotential at 10 mA cm⁻² and Tafel slope with previously reported catalysts. (d) Corresponding Tafel slope. (e) C_{dl} values, (f) Nyquist diagrams, and (g) TOF values of Ni NDC-Co/CP, NiCo NDC/CP, and Ni NDC/CP. (h) Chronopotentiometry curve of Ni NDC-Co/CP at 100 mA cm⁻².

the OER performance, where a larger ECSA implies more available active sites during the OER process. ECSA was identified by measuring the C_{dl} value in the CV curve of the nonfaradaic potential region with different scan rates (Figure S4). In Figure 4e, Ni NDC-Co/CP exhibits a larger C_{dl} (5.8 mF cm⁻²) compared to Ni NDC/CP (0.58 mF cm⁻²) and NiCo NDC/CP (5.3 mF cm⁻²), suggesting that Co doping and Co₃O₄ modification improved the intrinsic activity of Ni NDC. To further mitigate the influence of ECSA on the OER performance, ECSA-normalized LSV curves were conducted and depicted in Figure S7. The results indicated that Ni NDC-Co/CP exhibited the most favorable intrinsic OER performance among the samples. Ionic resistance and transport resistance are critical factors influencing the electrocatalytic activity of OER. Therefore, the charge-transfer kinetics of the catalyst were further evaluated by measuring electrochemical impedance spectroscopy (EIS). The Nyquist plot of the electrode and the associated equivalent circuit model are shown in Figure 4f. Here, R_s represents the solution resistance of the electrolyte, R_{ct} denotes the charge-transfer resistance, and the constant-phase element (CPE) is related to the intrinsic activity and geometry of the catalyst.⁵³ In comparison to Ni NDC/CP (R_{ct} = 2.86 Ω) and NiCo NDC/CP (R_{ct} = 1.98 Ω), Ni NDC-Co/CP demonstrates a lower charge-transfer resistance (R_{ct} = 1.74 Ω), indicating the fastest charge-transfer kinetics. Additionally, turnover frequency (TOF), reflecting the number of O₂ molecules delivered per second per active site, is considered one of the most meaningful parameters for judging the intrinsic activity of catalysts.⁵⁴ The calculated TOF for the prepared catalysts follows the order: Ni NDC-Co/CP > NiCo NDC/CP > Ni NDC/CP (Figure 4g).

Based on these results, the enhanced OER performance exhibited by Ni NDC-Co/CP can be attributed to two key factors. First, Co doping contributes to the improved catalytic performance.⁵⁵ Second, the presence of Co₃O₄ modification on the Ni NDC surface facilitates the creation of more accessible active sites, thereby accelerating electron-transfer kinetics and enhancing its intrinsic activity. Long-term stability is also an essential criterion for evaluating catalysts. As shown in Figure 4h, Ni NDC-Co/CP exhibits remarkable stability, maintaining a voltage retention rate of over 98% in a current density over 100 h at 100 mA cm⁻², thus confirming its exceptional stability.

Leveraging the exceptional OER performance of Ni NDC-Co/CP, a water-splitting device was prepared to evaluate its electrocatalytic performance, utilized by Ni NDC-Co/CP as the anode and Pt/C/CP as the cathode (Figure 5a). At high current densities, the polarization curves exhibit slight instability, primarily due to the rapid formation of hydrogen bubbles at the electrode surface. As depicted in Figure 5b, the Ni NDC-Co/CP⁽⁺⁾||Pt/C/CP⁽⁻⁾ configuration exhibits a cell voltage of 1.52 and 1.63 V at 10 and 100 mA cm⁻², respectively, slightly lower than that of commercial RuO₂/CP⁽⁺⁾||Pt/C/CP⁽⁻⁾ and other previously published catalysts (Figure 5c, Table S3). Furthermore, the chronopotentiometry curve of Ni NDC-Co/CP⁽⁺⁾||Pt/C/CP⁽⁻⁾ at 100 mA cm⁻² was maintained for more than 70 h without significant recession (Figure 5d), attesting to its high durability for overall water splitting. Notably, during the stability test, O₂ and H₂ bubbles were observed on the anode and cathode surfaces, respectively, further confirming the successful electrochemical water splitting (inset in Figure 5d).

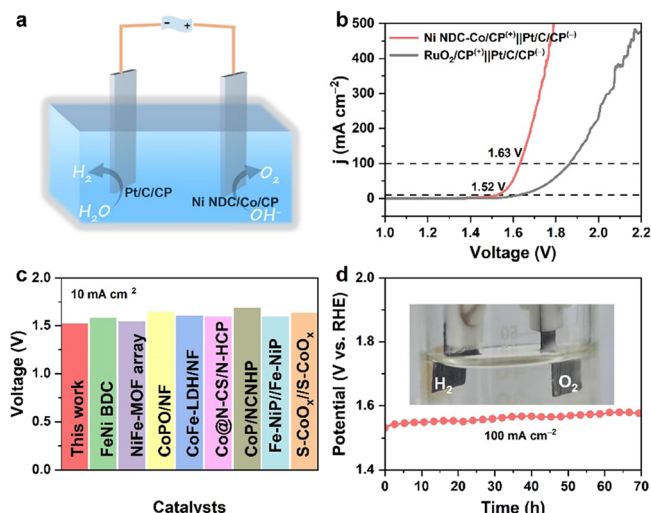


Figure 5. (a) Schematic diagram of the overall water splitting electrolyzer, (b) comparison of the polarization curves of Ni NDC-Co/CP⁽⁺⁾||Pt/C/CP⁽⁻⁾ and the RuO₂/CP⁽⁺⁾||Pt/C/CP⁽⁻⁾ at high currents in 1.0 M KOH, (c) comparing cell voltages with the recently reported electrolyzers at 10 mA cm⁻² in 1.0 M KOH, and (d) long-term stability test of Ni NDC-Co/CP⁽⁺⁾||Pt/C/CP⁽⁻⁾ at 100 mA cm⁻² in 1.0 M KOH.

Examining the microstructure and surface species evolution after the OER reaction is crucial for elucidating the catalytic mechanism. The XRD pattern indicates the disappearance of characteristic MOF peaks (Figure 6a), while newly emerged peaks can be attributed to NiOOH (PDF# 06–0075) and CoOOH (PDF# 07–0169).²⁸ Following the stability test, the catalyst retained its nanosheet morphology, as evidenced by the corresponding HR-TEM images revealing distinct lattice

stripes with spacings of 0.21 and 0.43 nm, consistent with the crystal planes of NiOOH (105) and CoOOH (003), respectively (Figures 6b,c and S8). EDX mapping demonstrates a uniform distribution of O, Ni, and Co elements after the OER stability testing (Figure S9).

Post OER stabilization, the surface XPS of the Ni NDC-Co/CP catalyst reveals a change in the area ratio of Ni³⁺/Ni²⁺ in the Ni 2p spectrum from 0.29 to 0.35, indicating the generation of more Ni³⁺ species (Figure 6d). Similarly, for the Co 2p spectra, the area ratio of Co³⁺/Co²⁺ increases to 0.99, illustrating the formation of Co oxide/hydroxides during the OER process (Figure 6e).^{56,57} Prior studies suggest that the high-valence Ni/Co not only promotes the occurrence of active phases in metal oxyhydroxides but also optimizes the electronic structure of the oxyhydroxides, accelerating OER kinetics.^{58,59}

In situ Raman was employed to verify the transformation mechanism of Ni NDC-Co/CP during the OER process in the potential range from 1.1 to 1.6 V with an interval of 0.1 V (Figure 6f). In the potential range 1.1–1.3 V (vs. RHE, 1.0 M KOH), the peak at around 680 cm⁻¹ corresponds to Co₃O₄, while the other peaks at around 494 and 520 cm⁻¹ represent Ni(OH)₂.⁶⁰ When the potential increased from 1.4 to 1.6 V, the characteristic peaks of Ni(OH)₂ and Co₃O₄ gradually disappeared, and two distinct signal peaks were detected at around 474 and 549 cm⁻¹, corresponding to the Ni/Co–O bond in Ni(Co)OOH, respectively.^{61,62} It is noteworthy that the peak at 1200 to 1800 cm⁻¹ can be attributed to the H₂NDC organic ligand. The gradual decomposition of H₂NDC can be observed from 1.1 to 1.6 V, further confirming the transformation of the Ni NDC-Co/CP surface into Ni(Co)OOH during the OER process, consistent with the XRD results.

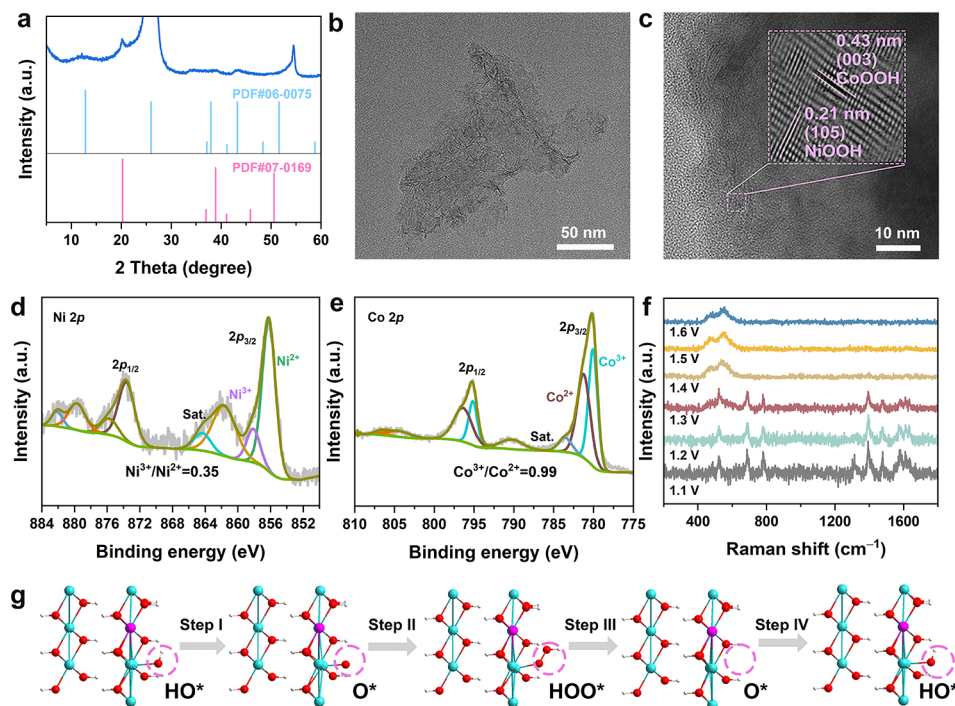


Figure 6. (a) XRD image, (b) TEM image, (c) HR-TEM image, (d) XPS of Ni 2p, and (e) XPS of Co 2p of Ni NDC-Co/CP after the OER stability test. (f) Electrochemical in situ Raman spectra of Ni NDC-Co/CP in the potential range of 1.1–1.6 V (vs RHE). (g) OER mechanistic illustration of Ni NDC-Co/CP.

The proposed catalytic mechanism is explained as follows (Figure 6g): Initially, OH⁻ is absorbed at the Ni/Co sites to form the Ni/Co–OH group (Step I). This is followed by the first deprotonation of the Ni/Co–OH group to form the Ni/Co–O group (Step II). As the reaction proceeds, the Ni/Co–O group combines with OH⁻ to form the superoxide species Ni/Co–OOH (Step III). Finally, the Ni/Co–OOH reacts with the OH⁻ and underwent deprotonation to produce O₂ and H₂O (Step IV).⁶³

Based on the above results, the excellent OER performance of Ni NDC-Co/CP can be attributed to several factors: (1) The presence of rough nanosheets facilitated by Co₃O₄, which are modified to enhance the contact area with the electrolyte, thereby expediting electron transfer under an electric field.⁶⁴ (2) The introduction of Co²⁺ leads to the generation of Co–O–Ni–O–Co units in Ni NDC-Co, optimizing the d-orbitals of Ni²⁺ and promoting the formation of Ni³⁺, thereby reducing the reaction energy barrier in the OER process.^{45,65} (3) In situ growth avoids the use of binders and preserves the catalytic capacity of the catalyst as much as possible.⁶⁶

CONCLUSIONS

In summary, we have prepared Ni NDC-Co/CP by using a solvothermal-assisted etching growth strategy. The unique nanosheet morphology, Co ion doping and Co₃O₄ modification on the surface of Ni NDC nanosheets identified as key contributors to its exceptional OER performance. As a result, the Ni NDC-Co/CP exhibits a low overpotential of 245 and 308 mV at 10 and 100 mA cm⁻², respectively, a Tafel slope of 49.1 mV dec⁻¹ and a long-term stability for 100 h at 100 mA cm⁻². In a water-splitting device, Ni NDC-Co/CP as the anode and Pt/C/CP as the cathode yielded cell voltages of 1.52 and 1.63 V at 10 and 100 mA cm⁻², respectively. Microstructural analyses confirmed the transformation of Ni NDC-Co/CP into Ni(Co)OOH during the OER process. Ni NDC-Co/CP emerges as a promising candidate for efficient electrochemical water splitting and provides an innovative approach to the design of high-performance MOF-based electrocatalysts.

ASSOCIATED CONTENT

Supporting Information

The Supporting Information is available free of charge at <https://pubs.acs.org/doi/10.1021/acs.inorgchem.4c00712>.

Details on the experimental method, characterization, electrochemical measurements, EIS study, true content of metal elements in different catalysts obtained by ICP-MS measurements, comparison of the OER activities of recently reported electrocatalysts, and summary of various catalytic electrodes for overall water splitting (PDF)

AUTHOR INFORMATION

Corresponding Authors

Tayirjan Taylor Isimjan – Saudi Arabia Basic Industries Corporation (SABIC) at King Abdullah University of Science and Technology (KAUST), Thuwal 23955-6900, Saudi Arabia; orcid.org/0000-0003-1735-481X; Email: isimjant@sabic.com

Dandan Cai – School of Chemical Engineering and Technology, Sun Yat-sen University, Zhuhai 519082, China; orcid.org/0000-0001-5004-7075; Email: caidandan86@163.com

Xiulin Yang – Guangxi Key Laboratory of Low Carbon Energy Materials, School of Chemistry and Pharmaceutical Sciences, Guangxi Normal University, Guilin 541004, China; orcid.org/0000-0003-2642-4963; Email: xlyang@gxnu.edu.cn

Authors

Haoran Yin – Guangxi Key Laboratory of Low Carbon Energy Materials, School of Chemistry and Pharmaceutical Sciences, Guangxi Normal University, Guilin 541004, China

Xinqiang Liu – Guangxi Key Laboratory of Low Carbon Energy Materials, School of Chemistry and Pharmaceutical Sciences, Guangxi Normal University, Guilin 541004, China

Lixia Wang – Guangxi Key Laboratory of Low Carbon Energy Materials, School of Chemistry and Pharmaceutical Sciences, Guangxi Normal University, Guilin 541004, China

Complete contact information is available at:

<https://pubs.acs.org/10.1021/acs.inorgchem.4c00712>

Author Contributions

The manuscript was written through contributions of all authors. All authors have given approval to the final version of the manuscript.

Notes

The authors declare no competing financial interest.

ACKNOWLEDGMENTS

This work was financially supported by the National Natural Science Foundation of China (No. 22068008, 21965005, and 52363028) and the Guangxi Province Natural Science Foundation (No. 2020GXNSFAA159104 and 2021GXNSFAA076001).

REFERENCES

- Deng, Z.; Sun, Z.; Li, Y.; Pei, J.; Chen, W. Electrochemical Oxygen Evolution Performance of Nitrogen-Doped Ultra-Thin Carbon Nanosheets Composite Ru₁Co Single Atom Alloy Catalysts. *Chin. J. Chem.* **2024**, *42*, 973–979.
- Shang, H.; Zhou, X.; Dong, J.; Li, A.; Zhao, X.; Liu, Q.; Lin, Y.; Pei, J.; Li, Z.; Jiang, Z.; Zhou, D.; Zheng, L.; Wang, Y.; Zhou, J.; Yang, Z.; Cao, R.; Sarangi, R.; Sun, T.; Yang, X.; Zheng, X.; Yan, W.; Zhuang, Z.; Li, J.; Chen, W.; Wang, D.; Zhang, J.; Li, Y. Engineering unsymmetrically coordinated Cu-S₁N₃ single atom sites with enhanced oxygen reduction activity. *Nat. Commun.* **2020**, *11* (1), 3049.
- Karmakar, A.; Karthick, K.; Sankar, S. S.; Kumaravel, S.; Madhu, R.; Kundu, S. A vast exploration of improvising synthetic strategies for enhancing the OER kinetics of LDH structures: a review. *J. Mater. Chem. A* **2021**, *9* (3), 1314–1352.
- Chen, W.; Wu, B.; Wang, Y.; Zhou, W.; Li, Y.; Liu, T.; Xie, C.; Xu, L.; Du, S.; Song, M.; Wang, D.; Liu, Y.; Li, Y.; Liu, J.; Zou, Y.; Chen, R.; Chen, C.; Zheng, J.; Li, Y.; Chen, J.; Wang, S. Deciphering the alternating synergy between interlayer Pt single-atom and NiFe layered double hydroxide for overall water splitting. *Energy Environ. Sci.* **2021**, *14* (12), 6428–6440.
- Bai, Y.; Wu, Y.; Zhou, X.; Ye, Y.; Nie, K.; Wang, J.; Xie, M.; Zhang, Z.; Liu, Z.; Cheng, T.; Gao, C. Promoting nickel oxidation state transitions in single-layer NiFeB hydroxide nanosheets for efficient oxygen evolution. *Nat. Commun.* **2022**, *13* (1), 6094.
- Qin, Y.; Cao, B.; Zhou, X.-Y.; Xiao, Z.; Zhou, H.; Zhao, Z.; Weng, Y.; Lv, J.; Liu, Y.; He, Y.-B.; Kang, F.; Li, K.; Zhang, T.-Y. Orthorhombic (Ru, Mn)₂O₃: A superior electrocatalyst for acidic oxygen evolution reaction. *Nano Energy* **2023**, *115*, No. 108727.
- Liang, Q.-M.; Wang, X.; Wan, X.-W.; Lin, L.-X.; Geng, B.-J.; Tian, Z.-Q.; Yang, Y. Opportunities and challenges of strain

- engineering for advanced electrocatalyst design. *Nano Research* **2023**, *16* (7), 8655–8669.
- (8) Zhang, H.; Bi, Z.; Sun, P.; Chen, A.; Wagberg, T.; Hu, X.; Liu, X.; Jiang, L.; Hu, G. Dense Crystalline/Amorphous Phosphides/Oxides Interfacial Sites for Enhanced Industrial-Level Large Current Density Seawater Oxidation. *ACS Nano* **2023**, *17* (16), 16008–16019.
- (9) Li, N.; Zhang, L.; Wang, Y.; Zhou, S.; Zhang, Y.; Abdulkayum, A.; Jin, Z.; Zhang, H.; Hu, G. Effect of in-plane Mott-Schottky on the hydroxyl deprotonation in $\text{MoS}_2/\text{Co}_3\text{S}_4/\text{NC}$ heterostructure for efficient overall water splitting. *J. Colloid Interface Sci.* **2023**, *649*, 125–131.
- (10) Pei, J.; Yang, L.; Lin, J.; Zhang, Z.; Sun, Z.; Wang, D.; Chen, W. Integrating Host Design and Tailored Electronic Effects of Yolk-Shell Zn-Mn Diatomic Sites for Efficient CO_2 Electroreduction. *Angew. Chem., Int. Ed.* **2024**, *63* (3), No. e202316123.
- (11) Chen, L.; Xu, Q. Metal-Organic Framework Composites for Catalysis. *Matter* **2019**, *1* (1), 57–89.
- (12) Xue, J. Y.; Li, C.; Li, F. L.; Gu, H. W.; Braunstein, P.; Lang, J. P. Recent advances in pristine tri-metallic metal-organic frameworks toward the oxygen evolution reaction. *Nanoscale* **2020**, *12* (8), 4816–4825.
- (13) Liu, Y.; Li, X.; Zhang, S.; Wang, Z.; Wang, Q.; He, Y.; Huang, W.; Sun, Q.; Zhong, X.; Hu, J.; Guo, X.; Lin, Q.; Li, Z.; Zhu, Y.; Chueh, C.; Chen, C.; Xu, Z.; Zhu, Z. Molecular Engineering of Metal-Organic Frameworks as Efficient Electrochemical Catalysts for Water Oxidation. *Adv. Mater.* **2023**, *35* (22), No. e2300945.
- (14) Wang, H. F.; Chen, L.; Pang, H.; Kaskel, S.; Xu, Q. MOF-derived electrocatalysts for oxygen reduction, oxygen evolution and hydrogen evolution reactions. *Chem. Soc. Rev.* **2020**, *49* (5), 1414–1448.
- (15) Beglau, T. H. Y.; Rademacher, L.; Oestreich, R.; Janiak, C. Synthesis of Ketjenblack Decorated Pillared Ni(Fe) Metal-Organic Frameworks as Precursor Electrocatalysts for Enhancing the Oxygen Evolution Reaction. *Molecules* **2023**, *28* (11), 4464.
- (16) Ding, J.; Guo, D.; Wang, N.; Wang, H.; Yang, X.; Shen, K.; Chen, L.; Li, Y. Defect Engineered Metal-Organic Framework with Accelerated Structural Transformation for Efficient Oxygen Evolution Reaction. *Angew. Chem., Int. Ed.* **2023**, *62* (43), No. e202311909.
- (17) Chu, H.; Li, R.; Feng, P.; Wang, D.; Li, C.; Yu, Y.; Yang, M. Ligands Defect-Induced Structural Self-Reconstruction of Fe–Ni–Co-Hydroxyl Oxides with Crystalline/Amorphous Heterophase from a 2D Metal–Organic Framework for an Efficient Oxygen Evolution Reaction. *ACS Catal.* **2024**, *14*, 1553–1566.
- (18) Zhao, S.; Tan, C.; He, C.-T.; An, P.; Xie, F.; Jiang, S.; Zhu, Y.; Wu, K.-H.; Zhang, B.; Li, H.; Zhang, J.; Chen, Y.; Liu, S.; Dong, J.; Tang, Z. Structural transformation of highly active metal–organic framework electrocatalysts during the oxygen evolution reaction. *Nat. Energy* **2020**, *5* (11), 881–890.
- (19) Ni, C.; Zheng, H.; Liu, W.; Wu, L.; Li, R.; Zhou, K.; Zhang, W. Linker Defects in Metal–Organic Frameworks for the Construction of Interfacial Dual Metal Sites with High Oxygen Evolution Activity. *Adv. Funct. Mater.* **2023**, *33* (25), No. 2301075.
- (20) Zhao, S. W. Y.; Dong, J.; He, C.-T.; Yin, H.; An, P.; Zhao, K.; Zhang, X.; Gao, C.; Zhang, L.; Lv, J.; Wang, J.; Zhang, J.; Khattak, A. M.; Khan, N. A.; Wei, Z.; Zhang, J.; Liu, S.; Zhao, H.; Tang, Z. Ultrathin metal–organic framework nanosheets for electrocatalytic oxygen evolution. *Nat. Energy* **2016**, *1*, No. 16184.
- (21) Shabbir, B.; Drissi, N.; Jabbour, K.; Gassoumi, A.; Alharbi, F. F.; Manzoor, S.; Ashiq, M. F.; Alburaih, H. A.; Ehsan, M. F.; Ashiq, M. N. Development of Mn-MOF/CuO composites as platform for efficient electrocatalytic OER. *Fuel* **2023**, *341*, No. 127638.
- (22) Xu, C.; Fang, R.; Luque, R.; Chen, L.; Li, Y. Functional metal–organic frameworks for catalytic applications. *Coord. Chem. Rev.* **2019**, *388*, 268–292.
- (23) Zhang, H.; Chen, A.; Bi, Z.; Wang, X.; Liu, X.; Kong, Q.; Zhang, W.; Mai, L.; Hu, G. MOF-on-MOF-Derived Ultrafine $\text{Fe}_2\text{P-Co}_2\text{P}$ Heterostructures for High-Efficiency and Durable Anion Exchange Membrane Water Electrolyzers. *ACS Nano* **2023**, *17* (23), 24070–24079.
- (24) Zheng, S.; Guo, X.; Xue, H.; Pan, K.; Liu, C.; Pang, H. Facile one-pot generation of metal oxide/hydroxide@metal-organic framework composites: highly efficient bifunctional electrocatalysts for overall water splitting. *Chem. Commun.* **2019**, *55* (73), 10904–10907.
- (25) Liu, M.; Min, K. A.; Han, B.; Lee, L. Y. S. Interfacing or Doping? Role of Ce in Highly Promoted Water Oxidation of NiFe-Layered Double Hydroxide. *Adv. Energy Mater.* **2021**, *11* (33), No. 2101281.
- (26) Li, Z.; Gao, R.; Feng, M.; Deng, Y. P.; Xiao, D.; Zheng, Y.; Zhao, Z.; Luo, D.; Liu, Y.; Zhang, Z.; Wang, D.; Li, Q.; Li, H.; Wang, X.; Chen, Z. Modulating Metal–Organic Frameworks as Advanced Oxygen Electrocatalysts. *Adv. Energy Mater.* **2021**, *11* (16), No. 2003291.
- (27) Hong, Q.; Wang, Y.; Wang, R.; Chen, Z.; Yang, H.; Yu, K.; Liu, Y.; Huang, H.; Kang, Z.; Menezes, P. W. In Situ Coupling of Carbon Dots with Co-ZIF Nanoarrays Enabling Highly Efficient Oxygen Evolution Electrocatalysis. *Small* **2023**, *19* (31), No. e2206723.
- (28) Jia, Z.; Yuan, Y.; Zhang, Y.; Lyu, X.; Liu, C.; Yang, X.; Bai, Z.; Wang, H.; Yang, L. Optimizing 3d spin polarization of CoOOH by in situ Mo doping for efficient oxygen evolution reaction. *Carbon Energy* **2023**, *6*, No. e418.
- (29) Liu, Y.; Wang, Y.; Wang, H.; Zhao, P.; Hou, H.; Guo, L. Acetylene black enhancing the electrochemical performance of NiCo-MOF nanosheets for supercapacitor electrodes. *Appl. Surf. Sci.* **2019**, *492*, 455–463.
- (30) Guo, Y.; Jia, K.; Dai, F.; Liu, Y.; Zhang, C.; Su, J.; Wang, K. Hierarchical porous tri-metallic NiCoFe-Se/CFP derived from Ni-Co-Fe Prussian blue analogues as efficient electrocatalyst for oxygen evolution reaction. *J. Colloid Interface Sci.* **2023**, *642*, 638–647.
- (31) Xu, H.; Xu, Z. A microporous coordination polymer of 2,6-Naphthalenedicarboxylate and cobalt(II) showing reversible structural and functional transformation. *Microporous Mesoporous Mater.* **2012**, *157*, 33–36.
- (32) Rani, B. J.; Raj, S. P.; Saravanakumar, B.; Ravi, G.; Ganesh, V.; Ravichandran, S.; Yuvakkumar, R. Controlled synthesis and electrochemical properties of Ag-doped Co_3O_4 nanorods. *Int. J. Hydrogen Energy* **2017**, *42* (50), 29666–29671.
- (33) Liang, J.; Gao, X.; Xu, K.; Lu, J.; Liu, D.; Zhao, Z.; Tse, E. C. M.; Peng, Z.; Zhang, W.; Liu, J. Unraveling the Asymmetric O horizontal line O Radical Coupling Mechanism on Ru horizontal line O horizontal line Co for Enhanced Acidic Water Oxidation. *Small* **2023**, *19* (45), No. e2304889.
- (34) Wang, Q.; Wei, F.; Manoj, D.; Zhang, Z.; Xiao, J.; Zhao, X.; Xiao, F.; Wang, H.; Wang, S. In situ growth of Fe(II)-MOF-74 nanoarrays on nickel foam as an efficient electrocatalytic electrode for water oxidation: a mechanistic study on valence engineering. *Chem. Commun.* **2019**, *55* (75), 11307–11310.
- (35) Yang, L.; Zhu, G.; Wen, H.; Guan, X.; Sun, X.; Feng, H.; Tian, W.; Zheng, D.; Cheng, X.; Yao, Y. Constructing a highly oriented layered MOF nanoarray from a layered double hydroxide for efficient and long-lasting alkaline water oxidation electrocatalysis. *J. Mater. Chem. A* **2019**, *7* (15), 8771–8776.
- (36) Xu, C.; Yang, X.; Li, S.; Li, K.; Xi, B.; Han, Q.-W.; Wu, Y.-P.; Wu, X.-Q.; Chi, R.-a.; Li, D.-S. Modulating the electronic configuration of Co species in MOF/MXene nanosheet derived Co-based mixed spinel oxides for an efficient oxygen evolution reaction. *Inorg. Chem. Front.* **2022**, *10* (1), 85–92.
- (37) Zhao, X.; Liu, Y.; Wang, J.; Qian, L.; Yao, L.; Chen, Z.; Cai, Q.; Xing, X.; Wu, Z. Modulating the Hydrothermal Synthesis of Co_3O_4 and CoOOH Nanoparticles by H_2O_2 Concentration. *Inorg. Chem.* **2019**, *58* (10), 7054–7061.
- (38) Wang, D.; Li, Q.; Han, C.; Lu, Q.; Xing, Z.; Yang, X. Atomic and electronic modulation of self-supported nickel-vanadium layered double hydroxide to accelerate water splitting kinetics. *Nat. Commun.* **2019**, *10* (1), 3899.
- (39) Wang, X.; Xiao, H.; Li, A.; Li, Z.; Liu, S.; Zhang, Q.; Gong, Y.; Zheng, L.; Zhu, Y.; Chen, C.; Wang, D.; Peng, Q.; Gu, L.; Han, X.; Li,

- J.; Li, Y. Constructing NiCo/Fe₃O₄ Heteroparticles within MOF-74 for Efficient Oxygen Evolution Reactions. *J. Am. Chem. Soc.* **2018**, *140* (45), 15336–15341.
- (40) Hou, X.; Jiang, T.; Xu, X.; Wang, X.; Zhou, J.; Xie, H.; Liu, Z.; Chu, L.; Huang, M. Coupling of NiFe-Based Metal-Organic Framework Nanosheet Arrays with Embedded Fe-Ni₃S₂ Clusters as Efficient Bifunctional Electrocatalysts for Overall Water Splitting. *Chin. J. Struct. Chem.* **2022**, *41*, 2207074–2207080.
- (41) Lu, H.-S.; Zhang, H.; Liu, R.; Zhang, X.; Zhao, H.; Wang, G. Macroscale cobalt-MOFs derived metallic Co nanoparticles embedded in N-doped porous carbon layers as efficient oxygen electrocatalysts. *Appl. Surf. Sci.* **2017**, *392*, 402–409.
- (42) Qiu, Y.; Liu, J.; Sun, M.; Yang, J.; Liu, J.; Zhang, X.; Liu, X.; Zhang, L. Rational Design of Electrocatalyst with Abundant Co/MoN Heterogeneous Domains for Accelerating Hydrogen Evolution Reaction. *Chin. J. Struct. Chem.* **2022**, *41*, 2207040–2207045.
- (43) Zhang, B.; Shang, X.; Jiang, Z.; Song, C.; Maiyalagan, T.; Jiang, Z.-J. Atmospheric-Pressure Plasma Jet-Induced Ultrafast Construction of an Ultrathin Nonstoichiometric Nickel Oxide Layer with Mixed Ni³⁺/Ni²⁺ Ions and Rich Oxygen Defects as an Efficient Electrocatalyst for Oxygen Evolution Reaction. *ACS Appl. Energy Mater.* **2021**, *4* (5), 5059–5069.
- (44) Wang, Y.; Tao, S.; Lin, H.; Han, S.; Zhong, W.; Xie, Y.; Hu, J.; Yang, S. NaBH₄ induces a high ratio of Ni³⁺/Ni²⁺ boosting OER activity of the NiFe LDH electrocatalyst. *RSC Adv.* **2020**, *10* (55), 33475–33482.
- (45) Li, J.; Wang, L.; He, H.; Chen, Y.; Gao, Z.; Ma, N.; Wang, B.; Zheng, L.; Li, R.; Wei, Y.; Xu, J.; Xu, Y.; Cheng, B.; Yin, Z.; Ma, D. Interface construction of NiCo LDH/NiCoS based on the 2D ultrathin nanosheet towards oxygen evolution reaction. *Nano Res.* **2022**, *15* (6), 4986–4995.
- (46) Zhao, L.; Yan, J.; Huang, H.; Du, X.; Chen, H.; He, X.; Li, W.; Fang, W.; Wang, D.; Zeng, X.; Dong, J.; Liu, Y. Regulating Electronic Structure of Bimetallic NiFe-THQ Conductive Metal–Organic Frameworks to Boost Catalytic Activity for Oxygen Evolution Reaction. *Adv. Funct. Mater.* **2023**, *34* (9), No. 2310902.
- (47) Liu, X.; Cao, S.; Li, J.; Wang, Y.; Xue, W.; Liu, G. Protective Cerium Oxide Coating Promoted Ce-Doping and Reconstruction of High-Valence NiFe Sulfide toward Robust Overall Water Splitting. *Small* **2023**, *19* (50), No. e2304652.
- (48) Lee, W. H.; Han, M. H.; Ko, Y. J.; Min, B. K.; Chae, K. H.; Oh, H. S. Electrode reconstruction strategy for oxygen evolution reaction: maintaining Fe-CoOOH phase with intermediate-spin state during electrolysis. *Nat. Commun.* **2022**, *13* (1), 605.
- (49) Nagappan, S.; Karmakar, A.; Madhu, R.; Dhandapani, N. H.; Bera, K.; De, A.; Kundu, S. Electronically Modified Ce³⁺ Ion Doped 2D NiFe-LDH Nanosheets over a 1D Microfiber: A High-Performance Electrocatalyst for Overall Water Splitting. *ACS Appl. Energy Mater.* **2022**, *5* (10), 12768–12781.
- (50) Wei, C.; Feng, Z.; Scherer, G. G.; Barber, J.; Shao-Horn, Y.; Xu, Z. J. Cations in Octahedral Sites: A Descriptor for Oxygen Electrocatalysis on Transition-Metal Spinel. *Adv. Mater.* **2017**, *29* (23), No. 1606800.
- (51) Feng, K.; Song, R.; Xu, J.; Chen, Y.; Lu, C.; Li, Y.; Hofer, W.; Lin, H.; Kang, Z.; Zhong, J. The S-Fe(Ni) sub-surface active sites for efficient and stable overall water splitting. *Appl. Catal. B Environ.* **2023**, *325*, No. 122365.
- (52) Liu, S.; Xing, Y.; Zhou, Z.; Yang, Y.; Li, Y.; Xiao, X.; Wang, C. Heterostructure iron selenide/cobalt phosphide films grown on nickel foam for oxygen evolution. *J. Mater. Chem. A* **2023**, *11* (15), 8330–8341.
- (53) Jorcin, J.-B.; Orazem, M. E.; Pébère, N.; Tribollet, B. CPE analysis by local electrochemical impedance spectroscopy. *Electrochim. Acta* **2006**, *51* (8), 1473–1479.
- (54) Shi, Y.; Zhou, S.; Liu, J.; Zhang, X.; Yin, J.; Zhan, T.; Yang, Y.; Li, G.; Lai, J.; Wang, L. An integrated amorphous cobalt phosphoselenide electrocatalyst with high mass activity boosts alkaline overall water splitting. *Appl. Catal. B Environ.* **2024**, *341*, No. 123326.
- (55) Pei, Z.; Lu, X. F.; Zhang, H.; Li, Y.; Luan, D.; Lou, X. W. D. Highly Efficient Electrocatalytic Oxygen Evolution Over Atomically Dispersed Synergistic Ni/Co Dual Sites. *Angew. Chem., Int. Ed.* **2022**, *61* (40), No. e202207537.
- (56) Li, Y.; Gao, Z.; Bao, H.; Zhang, B.; Wu, C.; Huang, C.; Zhang, Z.; Xie, Y.; Wang, H. Amorphous nickel-cobalt bimetal-organic framework nanosheets with crystalline motifs enable efficient oxygen evolution reaction: Ligands hybridization engineering. *J. Energy Chem.* **2021**, *53*, 251–269.
- (57) Lu, Z.; Wang, K.; Cao, Y.; Li, Y.; Jia, D. Amino-functionalized iron-based MOFs modified with 2D FeCo(OH) hybrids for boosting oxygen evolution. *J. Alloys Compd.* **2021**, *871*, No. 159580.
- (58) Zhao, T.; Zhong, D.; Hao, G.; Liu, G.; Li, J.; Zhao, Q. Porous CoNiOOH nanosheets derived from the well-mixed MOFs as stable and highly efficient electrocatalysts for water oxidation. *Int. J. Hydrogen Energy* **2022**, *47* (77), 32928–32939.
- (59) Zhang, Y.; Ma, D.; Lei, Y.; Zhu, T.; Hu, J.; Tang, Y.; Chen, Z.; Huang, J.; Lai, Y.; Lin, Z. Markedly enhanced hydrogen production in wastewater via ammonia-mediated metal oxyhydroxides active sites on bifunctional electrocatalysts. *Nano Energy* **2023**, *117*, No. 108896.
- (60) Lai, W.; Ge, L.; Li, H.; Deng, Y.; Xu, B.; Ouyang, B.; Kan, E. In situ Raman spectroscopic study towards the growth and excellent HER catalysis of Ni/Ni(OH)₂ heterostructure. *Int. J. Hydrogen Energy* **2021**, *46* (53), 26861–26872.
- (61) Wang, B.; Han, X.; Guo, C.; Jing, J.; Yang, C.; Li, Y.; Han, A.; Wang, D.; Liu, J. Structure inheritance strategy from MOF to edge-enriched NiFe-LDH array for enhanced oxygen evolution reaction. *Appl. Catal. B Environ.* **2021**, *298*, No. 120580.
- (62) Yao, N.; Wang, G.; Jia, H.; Yin, J.; Cong, H.; Chen, S.; Luo, W. Intermolecular Energy Gap-Induced Formation of High-Valent Cobalt Species in CoOOH Surface Layer on Cobalt Sulfides for Efficient Water Oxidation. *Angew. Chem., Int. Ed.* **2022**, *61* (28), No. e202117178.
- (63) Chen, P.; Hu, X. High-Efficiency Anion Exchange Membrane Water Electrolysis Employing Non-Noble Metal Catalysts. *Adv. Energy Mater.* **2020**, *10* (39), No. 2002285.
- (64) Wang, W.; Xu, H.; Zhao, W.; Zhao, J.; Jiang, M.; Liu, S.; Huang, W.; Zhao, Q. Porphyrin-assisted synthesis of hierarchical flower-like polypyrrole arrays based flexible electrode with high areal capacitance. *Chem. Eng. J.* **2022**, *428*, No. 131089.
- (65) Liu, J.; He, L.; Tao, Z.; Li, S.; Wang, C.; Zhang, Y.; Zhang, S.; Du, M.; Zhang, Z. Ferric Oxide Nanocrystals-Embedded Co/Fe-MOF with Self-Tuned d-Band Centers for Boosting Urea-Assisted Overall Water Splitting. *Small* **2023**, *20*, No. e2306273.
- (66) Tan, P.; Chen, B.; Xu, H.; Cai, W.; He, W.; Ni, M. In-situ growth of Co₃O₄ nanowire-assembled clusters on nickel foam for aqueous rechargeable Zn-Co₃O₄ and Zn-air batteries. *Appl. Catal. B Environ.* **2019**, *241*, 104–112.